High-pressure phase of $CeRu_2$: A magnetic superconductor with two charge states of Ru ions

A. V. Tsvyashchenko and L. N. Fomicheva
Vereshchagin Institute of High Pressure Physics, Russian Academy of Sciences, 142092 Troitsk, Moscow region, Russia

A. A. Sorokin, G. K. Ryasny, B. A. Komissarova, and L. G. Shpinkova
Skobeltsyn Institute of Nuclear Physics, Moscow State University, 119899 Moscow, Russia

K. V. Klementiev, A. V. Kuznetsov, and A. P. Menushenkov
Department of Quantum Electronics, Moscow Engineering Physics Institute, Kashirskoe shosse 31, 115409 Moscow, Russia

V. N. Trofimov
Joint Institute for Nuclear Research, Laboratory of Nuclear Problems, P.O. Box 79, Moscow, Russia

A. E. Primenko
Department of Low Temperature Physics, Moscow State University, 117234 Moscow, Russia

R. Cortes
Laboratoire pour l' Utilisation du Rayonnement Electromagnetique, 91405, Orsay, France
(Received 15 August 2001; revised manuscript received 4 December 2001; published 22 April 2002)

The intermetallic compounds $LaRu_2$ and $CeRu_2$, as well as several quasibinary systems $Ce_{1-x}La_xRu_2$, were synthesized at a pressure of 8 GPa. The x-ray diffraction data showed the pure cubic $C15$ structure for all samples. The x-ray absorption measurements gave the value 3.23 for the Ce valence. Time-differential perturbed angular correlation measurements with the ^{111}In-doped samples have shown (i) ^{111}In substituted for Ru; (ii) in $LaRu_2$ a single value of the quadrupole frequency $\nu_Q = 234$ MHz for the daughter ^{111}Cd nuclei was observed; (iii) in $CeRu_2$ two distinct equally populated sites for ^{111}Cd were revealed with $\nu_Q = 218$ and $\nu_Q = 153$ MHz. The low-temperature magnetic measurements showed that magnetic moments about $0.3\mu_B$ per formula unit are inherent in all samples and indicated at a coexistence of superconductivity and magnetic ordering. In particular, the magnetic and superconducting correlations are developing, most probably, in the same system of ruthenium $4d$ electrons.

DOI: 10.1103/PhysRevB.65.174513 PACS number(s): 74.25.Ha, 74.62.Fj, 74.70.Ad, 75.20.Hr

I. INTRODUCTION

Strong electronic correlations induced by the presence of f electrons in lanthanide and actinide metallic compounds have been of permanent experimental and theoretical interest during last three decades. Though the f states in such compounds are located well below the Fermi level, their hybridization with electronic states of neighboring atoms (f-ligand hybridization[1]) determines their strong influence on the conduction-band states. Depending on the type and strength of the f-ligand hybridization and on the coordination number of the ligand atoms, the f electrons are either totally localized or partially localized and partially itinerant. In the first situation the system represents a nonmagnetic or magnetic Kondo lattice,[2] and in the latter case it exists in the so-called mixed-valence state.[3] Heavy-fermion behavior accompanied, at low temperatures, by superconductivity and magnetism is often observed in lanthanide and actinide compounds.[1,2,4–6]

Among cerium intermetallic systems, $CeRu_2$ is characterized by a high delocalization of the $4f$ electrons and by an intermediate cerium valence of 3.2–3.3.[7–10] Photoemission experiments[11–15] gave evidence of a strong hybridization of the Ce $4f$ and Ru $4d$ states. Band calculations predict the existence in $CeRu_2$ of a rather wide $4f$ band with about a 30% contribution of the f component into the density of states at the Fermi level.[16–18] The Fermi surface determined from the de Haas–van Alphen oscillations,[19] the electronic coefficient of the specific heat,[18,20,21] and the photoemission data[15] are consistent with an itinerant $4f$-band model. All these facts allow us to consider $CeRu_2$ as a typical example of a mixed-valence system.

$CeRu_2$ belongs to heavy-fermion superconductors with relatively low values of the temperature-independent magnetic susceptibility,[21] $\chi_0 = 5.9\times10^{-4}$ cm^3/mol, and linear electronic coefficient of the specific heat,[18,20–22] $\gamma = 23$–29 mJ/K^{2}mol (here and below we use mole assuming Avogadro number of formula units, i.e., $CeRu_2$). The cited values testify that no local moments are associated with the $4f$ electrons. At the same time, the magnetic, transport, and muon-spin-relaxation experiments indicated an antiferromagnetic ordering at $T = 40$–50 K.[23,24] An estimated magnetic moment $\mu \gtrsim 10^{-4}\mu_B$ (μ_B is the Bohr magneton) is consistent with a small value of the field-induced moment $\mu \simeq 4\times10^{-4}\mu_B$ observed in experiments with polarized neutrons and is associated with both cerium and ruthenium ions.[25] Below the temperature of the superconducting transition, $T_c = 6.2$ K, magnetic order still persists[23,24] making $CeRu_2$ a magnetic superconductor, similar to the heavy-fermion superconductors URu_2Si_2 and UPt_3 which exhibit a magnetic phase transition with a relatively large correlation

 ©2002 The American Physical Society

length and small magnetic moment $\mu \simeq (0.02–0.04)\mu_B$.[26]

Because of the intermediate valence state of cerium, its alloys with *d* metals often demonstrate properties differing from those of the alloys with three-valent rare-earth elements. Hence, in the present work we consider $CeRu_2$ in comparison with $LaRu_2$. The difference in their electronic structures and corresponding macroscopic properties is mostly due to the absence (La) or presence (Ce) of $4f$ electrons. For example, the critical temperature $T_c = 3.08$ K and the electronic contribution to the specific heat are lower in $LaRu_2$ as compared to $CeRu_2$.[20] Band calculations confirmed the significant role of ruthenium $4d$ electrons in the superconductivity of both compounds.[16–18,27]

Studying the solid solution $Ce_{1-x}La_xRu_2$ might elucidate the role and mechanism of the $4f$-$4d$ hybridization. Starting from the nonmagnetic metal $LaRu_2$, one passes through the Kondo-impurity and Kondo-lattice states in the intermediate compositions of $Ce_{1-x}La_xRu_2$ and finishes with the mixed-valence state in $CeRu_2$.[28]

$CeRu_2$ and $LaRu_2$ belong to the class of Laves phases with a cubic crystal structure of the $MgCu_2$ type[25,29] ($C15$) ($LaRu_2$ undergoes a structural transition below 30 K where it is no longer the $C15$ Laves phase).[29] The La impurity in $CeRu_2$ decreases the number of the $4f$ electrons and increases the lattice constant *a* since the ionic radius of lanthanum is greater than that of cerium. This, in turn, should affect the *f*-*d* hybridization which is strongly dependent on the *f*-ligand separation.[1]

The electronic properties of $Ce_{1-x}La_xRu_2$ are rather sensitive to doping and pressure.[28,29,30–32] For example, experiments by Hedo *et al.*[32] evidenced an electronic transition at a pressure of 5.5 GPa in $CeRu_2$.

As was shown earlier, the electronic structure of *f*-*d*-metal alloys could be different for samples crystallized at an ambient pressure and elevated pressure of several GPa. Due to different filling of the *f*-*d* bands, a metastable electronic state could be formed in samples prepared at high pressure. For example, in $GdNi_2$ synthesized at a pressure above 4 GPa, the Ni ions exhibited a charge state with the $3d$ population number $n_d < 10$, while for the samples synthesized at low pressure $n_d = 10$.[33]

Thus, depending on the synthesis pressure, alloys of the rare-earth elements and transition metals with almost filled *d* band could have different electronic *d* states. It is not yet clear whether the difference in the states is induced by changes in the density of electronic states caused by the lattice contraction (due to doping or pressure) or originates from changes in the hybridized *f*-*d* states near the Fermi level. Furthermore, the sensitivity of the lattice parameter to changes in the electronic structure should also be regarded.

In order to clarify the above questions we investigated samples of $CeRu_2$, $LaRu_2$, and quasibinary compounds $Ce_{1-x}La_xRu_2$ prepared at high pressure. We have performed magnetic measurements and studied electronic states of ions and the local crystalline structure. The following methods and techniques were applied: superconductiong quantum interference device (SQUID) magnetometry, time-differential perturbed angular $\gamma\gamma$ correlations, and x-ray absorption fine-structure spectroscopy (XAFS).

The paper is organized as follows. In the next section we discuss the sample preparation method and briefly describe the experimental techniques used. In Sec. III the experimental data are presented. We show that macroscopic properties and the state of the ruthenium ions are significantly affected by a high-pressure treatment while the crystal structure and the state of cerium ions are left unchanged. In Sec. IV we discuss the obtained data in the framework of the results of electronic band structure calculations for $CeRu_2$ and $LaRu_2$.[16–18,27]

II. EXPERIMENT

A. Sample preparation and analysis

The samples of $CeRu_2$, $LaRu_2$, and several compositions of the quasibinary system $Ce_{1-x}La_xRu_2$ were synthesized at a pressure of 8 GPa by a method as described by Tsvyashchenko.[34] The high pressure was generated in a chamber designed by Khvostantsev *et al.*[35] For the sample preparation a stoichiometric mixture of cerium ruthenium and lanthanum metals with chemical purity of 99.9%, 99.9%, and 99%, respectively, was melted, cooled down, and crystallized at high pressure in the NaCl envelope.

The composition of the samples was confirmed the by x-ray microanalysis. The x-ray diffraction measurements were performed using a 114-mm Debye-Scherrer chamber and a DRON-2 diffractometer with Ni-filtered Cu $K\alpha$ radiation. A NaCl inner reference standard was added for accurate determination of the lattice constants. All samples of $Ce_{1-x}La_xRu_2$ exhibited a single-phase structure of the cubic ($C15$) Laves phase type, in agreement with the data published for samples prepared at ambient pressure.[29] A sketch of the $C15$ crystal structure and lattice constants obtained are given in Fig. 1. In the lattice, both Ce and La occupy crystallographic sites with cubic point symmetry while Ru ions are located at vortices of tetrahedrons with threefold axial symmetry.

It is seen that the lattice constant dependence on the relative concentration is linear, indicating the mutual solubility of both intermetallics. Thus, in quasibinary systems, Ce and La ions should statistically substitute one another at random. The lattice constants for other RRu_2 Laves compounds (*R* stands for rare earths) are also shown in Fig. 1 for comparison.

A number of samples were annealed or remelted at normal pressure. All these samples showed the same lattice structure with the same lattice constant as prior to the thermal treatment. The appropriate measurements were carried out before and after the treatment.

Magnetization was studied in the temperature range $4.2\ \text{K} < T < 300$ K and magnetic field up to $H = 9$ kOe using the SQUID magnetometer designed by Trofimov.[36]

B. X-ray absorption measurements

Measurements of the x-ray absorption coefficient $\mu(E)$ as a function of energy *E* give information on the electronic structure and local space configuration of the atom specified

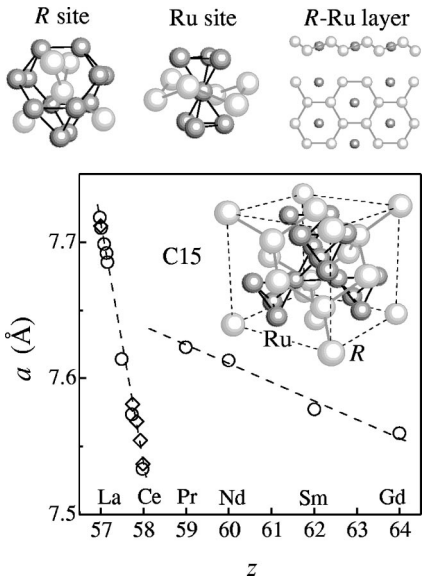

FIG. 1. Lattice parameter of cubic Laves-phase $R\mathrm{Ru}_2$ vs the number of rare-earth elements R and composition dependence of the lattice parameter for $\mathrm{Ce}_{1-x}\mathrm{La}_x\mathrm{Ru}_2$. In the inset the $C15$ lattice is shown. The structure of the R-Ru layers and surroundings of R and Ru sites are shown at the top of the figure. Circles are data from Ref. 29 for $\mathrm{Ce}_{1-x}\mathrm{La}_x\mathrm{Ru}_2$ and from Ref. 50 for other $R\mathrm{Ru}_2$. Diamonds are data obtained for $\mathrm{Ce}_{1-x}\mathrm{La}_x\mathrm{Ru}_2$ synthesized at 8 GPa. Dashed lines are guides for eyes.

by the chosen absorption edge.[37] The oscillatory extended structure above the edge contains information about the environmental parameters of the specified atom. The features of the x-ray absorption near-edge structure (XANES) are determined by the valence state of the absorbing atom and by the empty electronic states near and above the Fermi level. The extended x-ray absorption fine structure (EXAFS) contains the structural information.

The normalized EXAFS function $\chi(k)=\mu/\mu_0-1$ is obtained by subtracting the background $\mu_0(k)$ from the measured absorption coefficient $\mu(k)$. Here $k=\sqrt{2m_e(E-E_0)}/h$ is the photoelectron wave number and E_0 is the absorbing-atom edge energy. To obtain information on the local structure around the absorbing atom, the EXAFS function may be transformed as follows:

$$\chi(k)=\sum_r N_r \frac{|f(k)|}{kr^2}\sin(2kr+2\delta_c+\Phi)e^{-2\sigma^2k^2}, \qquad (1)$$

which can be fitted by varying the structural parameters. The latter are the interatomic distances r, the coordination numbers N_r, and the temperature-dependent rms fluctuation in bond lengths σ (Debye-Waller factor), which should also include effects due to structural disorder. In addition, $f(k)=|f(k)|e^{i\Phi(k)}$ is the backscattering amplitude and δ_c is absorbing-atom partial-wave phase shift of the final state. In the present work these latter values were calculated by the program FEFF8.1.[38]

The local crystal structure was inferred from the EXAFS spectra at the K Ru edge. Since the extended structure of the L_3 Ce edge is rather short because of the interference of the nearby L_2 Ce edge, only L_3 XANES was analyzed to deduce the cerium valence state.

X-ray absorption measurements have been performed in the transmission mode at LURE (Orsay, France) on the D-21 beamline using a double-crystal Si (311) monochromator. The energy resolution was about 2 eV for XANES measurements at 5 keV. Samples crushed into a fine powder were precipitated onto a microporous substrate in an amount corresponding to about two absorption lengths of the proper absorption edge. The low-temperature measurements were carried out with a liquid helium circulation cryostat. The temperature was regulated by the helium flow and measured with an accuracy of 1 K.

C. Time-differential perturbed angular $\gamma\gamma$ correlation

The method of time-differential perturbed angular correlations (TDPAC) of γ rays is one of the nuclear spectroscopic methods used to study the magnetic dipole and electric quadrupole interactions experienced by atomic nucleus with their electronic and ionic environment in condensed matter. The theory of perturbed angular correlations is described elsewhere (see, for example, Ref. 39).

The electric quadrupole hyperfine interaction (EQI) represents the interaction of a nuclear quadrupole moment Q of a probe atom with an electric field gradient (EFG) created by surrounding electrons and ions. The EFG is characterized by the main component V_{zz} and the asymmetry parameter η. The EQI parameters are sensitive to the local charge distribution and, in particular, to the symmetry of the probe-atom site.

In this work we performed TDPAC measurements using the well-known nuclear probe $^{111}\mathrm{In}/^{111}\mathrm{Cd}$ introduced into the lattice of $\mathrm{Ce}_{1-x}\mathrm{La}_x\mathrm{Ru}_2$ compounds synthesized at high pressure.

^{111}In decays into ^{111}Cd by electron capture with a half-life of 2.7 days. In the experiments, the well-known 172–247 keV γ-ray cascade proceeding via the 247 keV isomeric state in the daughter ^{111}Cd (spin $I=5/2$, half-life $T_{1/2}=85$ ns, quadrupole moment $Q=0.77$ b) is measured using a multidetector scintillation coincidence spectrometer.

The ^{111}In activity was produced via the $^{109}\mathrm{Ag}(\alpha,2n)^{111}\mathrm{In}$ reaction by irradiating a silver foil by the 32 MeV α beam of the cyclotron of the Nuclear Physics Institute, Moscow State University. Small pieces of the irradiated foil (1–2 mg) have been melted together with stoichiometric amounts of powdered Ru, Ce, and La (a total mass 500–600 mg) at a pressure of 8 GPa. One sample of $CeRu_2$ was also synthesized at a pressure of 5 GPa. The ingots were crushed and small bright fragments from the inner parts of the ingots were used for the TDPAC experiments.

After the ^{111}In activity practically decayed out, the x-ray diffraction of the samples was measured. All samples were of pure cubic $C15$ Laves phase structure.

TDPAC spectra were measured using a coincidence spectrometer with a time resolution of 1.8 ns. Assemblies of BaF_2-XP2020Q and NaI(Tl)-RCA7585 detectors were located in the horizontal plane, so that several coincidence

spectra $N(\vartheta,t)$ for different pairs of detectors, separated by an angle of $\vartheta=\pi/2$ or π, were collected simultaneously. The anisotropy spectra of the perturbed angular correlation were obtained for each combination of $N(\vartheta,t)$ spectra using the equation

$$R=-2\frac{N(\pi,t)-N(\pi/2,t)}{N(\pi,t)+2N(\pi/2,t)}=-A_{22}Q_2G_2(t), \qquad (2)$$

where $Q_2\approx 0.80$ is the solid-angle correction, $G_2(t)$ is the perturbation factor describing a nuclear spin precession due to a hyperfine interaction, and $A_{22}=-0.17$ is the unperturbed correlation coefficient for the $\gamma\gamma$ cascade used in ^{111}Cd.

All spectra were measured at room temperature and atmospheric pressure, i.e., in the paramagnetic state of the samples. Therefore, the observed perturbation of the angular correlation is due to a pure electric quadrupole interaction with a perturbation factor determined by the following equation (for the spin $I=5/2$ of the intermediate state of the γ-ray cascade and a polycrystalline sample):

$$G_2(t)=\sum_i p_i\sum_{l=0}^{3} a_l(\eta_i)\cos[\omega_l(\eta_i)t]\exp[-\Lambda_i\omega_l(\eta_i)t]. \qquad (3)$$

Here p_i are the relative populations of i inequivalent sites of probe atoms, a_l are the amplitude coefficients, and ω_l are the frequencies. The latter are functions of the EFG asymmetry parameter η and quadrupole frequency $\nu_Q=eQV_{zz}/h$. Here Λ is the relative half-width at half-maximum of the ν_Q distribution around the mean value assuming its Lorentzian shape. This distribution takes into account variations in the EFG parameters at different lattice sites caused by imperfections of the crystal lattice.

The EFG parameters were determined by least-squares fitting of the TDPAC spectra in accordance with Eq. (3) assuming one or several sites of probe atoms.

III. RESULTS

A. Mixed valence of Ce ions

Two samples of $CeRu_2$ synthesized at 8 GPa and one annealed at 850 °C for 4 h were studied by the XAFS methods. Figure 2 shows the experimental XANES spectra near the L_3 Ce absorption edge measured in the temperature range $7\ \text{K}\leqslant T\leqslant 300\ \text{K}$ for the as-cast and annealed samples. The pre-edge background was subtracted. As long as the near-edge structure is sensitive to the valence state of the absorbing atom,[40] this structure being practically identical for all measured spectra, one may conclude that the valence state of Ce is independent of both temperature and the thermal treatment of the samples.

The Ce valence was determined by the quantitative analysis of the XANES structure using the FEFF8.1 code.[38] At the first stage the absorption spectrum of monovalent Ce^{3+} was simulated. The self-consistent potential calculations were performed for a cluster of 17 atoms,[41] using the ground-state exchange correlation potential and the regular Laves-phase structure. The calculated signal was then convolved with the Gaussian with a width of 2.1 eV to account for the finite experimental resolution.

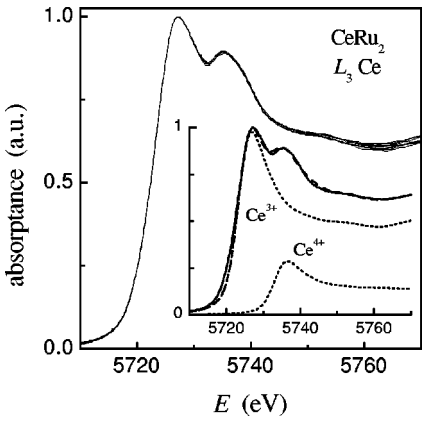

FIG. 2. L_3-edge Ce x-ray absorption measured at $T=7$, 50, 100, and 300 K for $CeRu_2$. Eight spectra normalized to unity at maximum are collected for both high-pressure synthesized and annealed samples. One of the spectra (solid line) and its fitting curve (dashed line) obtained by summation of the calculated spectra (dotted line) are shown in the inset.

The calculated profile of the Ce^{3+} spectrum was then shifted upwards in energy by 9.6 eV for simulation of the Ce^{4+} spectrum since the FEFF8.1 code is unable to calculate it correctly. The intensities of the two peaks (dotted curves in the inset of Fig. 2) were varied to obtain the best fit (dashed curve) of the experimental curve (solid curve). From this fit the cerium valence was determined as 3.23 ± 0.02 which is close to the estimation 3.2 obtained by x-ray photoelectron spectroscopy.[7]

We have also deduced the valence in a traditional way (see, for example, Ref. 42) used earlier to estimate the cerium valence in $CeRu_2$.[8,10] We have subtracted steplike background $\mu_0(E)$ from the measured absorption coefficient and fitted the absorption peaks from the Ce^{4+} and Ce^{3+} ions by two Gaussians. The ratio of areas of Gaussians is equal to the ratio of the fractions of Ce^{4+} and Ce^{3+} ions.[8] We have obtained a cerium valence of ~ 3.3 which in good agreement with the data previously estimated in XAFS analysis.[8,10] However, as follows from the simulation by the FEFF8.1 code, near the absorption edge the background energy dependence is more complex than stepwise, and hence the procedure described above is incorrect, giving only a rough estimation of the valence.

For the absorption spectra above the K Ru edge the extended fine structure was obtained in a standard way.[43] Figure 3 shows the modules of Fourier transform of the EXAFS signals at $T=7$ K for the as-cast and annealed samples. The two spectra and, subsequently, their Fourier transforms are practically identical. Thus, annealing induced only minor, if any, variations in the interatomic distances r and Debye-Waller factors σ^2 obtained by fitting the EXAFS signals. It should be stressed that the peaks in the Fourier spectra are well separated, evidencing the high quality of the crystal structure of both samples.

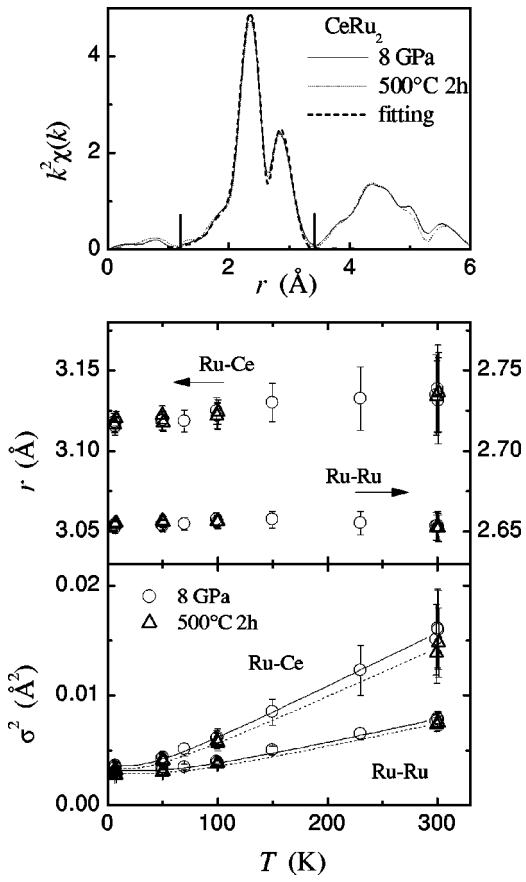

FIG. 3. On the analysis of the EXAFS *K* Ru spectra for $CeRu_2$. Upper panel: the Fourier transform of the EXAFS function obtained from the spectra measured at $T=7$ K for high-pressure synthesized and annealed $CeRu_2$ and the fit for the former. The fit was done over the *r* region specified by vertical marks. The Ru-Ru and Ru-Ce bond lengths (middle panel) and their Debye-Waller factors (lower panel) are inferred from the proper fits. The Einstein model theoretical curves are represented by solid and dotted lines for high-pressure synthesized and annealed samples, respectively.

The quantitative analysis of the EXAFS signals was carried out taking into account the contribution from the neighbors nearest to the absorbing ruthenium, i.e., six Ru atoms and six Ce atoms (see Ru-centered cluster in Fig. 1). The main double peak in the range 1.2–3.4 Å of the Fourier transform corresponds to the single-scattering paths within this cluster. Applying the standard single-electron EXAFS formula (1) with scattering amplitudes and phases calculated by the FEFF8.1 code, the experimental spectrum was fitted using five variable parameters: the threshold energy, distances of the Ru-Ru and Ru-Ce bond lengths, and their mean-square deviations σ^2. The coordination numbers of the nearest Ru and Ce shells were kept equal to 6.

The temperature dependence of bond lengths and Debye-Waller factors obtained by fitting the EXAFS spectra is shown in Fig. 3. The error bars were calculated taking into account all possible pair correlations between the fitting parameters. The uncertainties increased with temperature due to a significant decrease of the EXAFS signal with increasing thermal vibrations. It is seen that the $\sigma^2(T)$ dependences are well described by the function deduced from the Einstein model[44]; hence, the system is characterized as a harmonic one.

It is seen in Fig. 3 that the Ru-Ru bond length is practically independent of temperature, whereas the Ru-Ce bond length exhibits a normal temperature expansion. The lattice constants deduced from the obtained bond lengths are 7.51 ± 0.01 Å at 7 K and 7.53 ± 0.03 Å at 300 K.

The results of the XAFS studies show that the crystalline structure and the cerium valence do not differ for $CeRu_2$ synthesized at high and ambient pressure. In the present experiments we did not study the influence of doping by lanthanum on the cerium state, but Chaboy *et al.*[10] have not observed any variations in the cerium valence in $Ce_{1-x}La_xRu_2$ in a wide range of compositions $0 \leqslant x \leqslant 0.75$. This result seems to be strange since at low cerium content one expects localization of *f* states and a decrease of the cerium valence. To clarify this question we plan to continue XAFS experiments on $Ce_{1-x}La_xRu_2$.

From XAFS experiments we conclude that our high-pressure treatment neither modifies the lattice nor changes a filling of the localized *f* states. At the same time, as discussed in the next sections, it affects the electronic states of the ruthenium ions.

B. Electric field gradient at Ru sites

The TDPAC measurements were performed for six different samples of $CeRu_2$, three samples of $LaRu_2$, and two samples in the series $La_xCe_{1-x}Ru_2$ with $x=0.6$ and 0.2, synthesized at 8 GPa. The TDPAC spectra were reproducible and practically identical for different samples of each compound.

The TDPAC anisotropy spectrum for $LaRu_2$ is shown in Fig. 4(a). The spectrum can be fitted assuming a single lattice site occupied by the probe atoms, i.e., $p \simeq 1$. In whole, the perturbation pattern is similar to that observed by Devare *et al.*[45] with a sample prepared at ambient pressure. The fitting parameters obtained using Eq. (3) are presented in Table I. An approximation of the experimental data by Eq. (3) showed that the EQI is characterized by an axially symmetric EFG (η is close to zero) and a very narrow distribution, about 1%, of the quadrupole frequencies around the average value (see Table I). Thus, it can be assumed that probe atoms substitute the Ru sites with $3m$-point symmetry in the $LaRu_2$ lattice. The obtained quadrupole frequency of 234 MHz is about 8% lower than the value 254.4 MHz observed in Ref. 45, which may be attributed to the difference in the sample preparation procedures.[46]

The most prominent difference of the present results and those by Devare *et al.*[45] was observed for $CeRu_2$. One of our TDPAC spectra for $CeRu_2$ is shown in Fig. 4(d). There were detected two distinct, approximately equally populated, positions of the probe nuclei with different quadrupole frequencies (see Table I). The ν_Q value for site 1 is close to that observed for $LaRu_2$, indicating a similar charge distribution around the probe nuclei. In the error limits our ν_Q value for this site agrees with $\nu_Q = 220$ MHz determined in Ref. 45 for $CeRu_2$ prepared at ambient pressure.

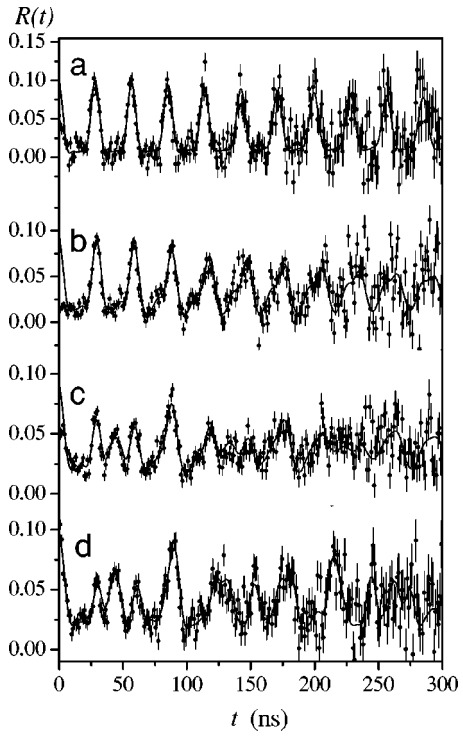

FIG. 4. ^{111}Cd-TDPAC spectra measured at room temperature and atmospheric pressure for samples synthesized at 8 GPa: (a) $LaRu_2$, (b) $La_{0.6}Ce_{0.4}Ru_2$, (c) $La_{0.2}Ce_{0.8}Ru_2$, and (d) $CeRu_2$.

The second site is also characterized by a well-determined EFG with a quite low value of the asymmetry parameter and an average value of the quadrupole frequency $\nu_Q = 152$ MHz.

The same two frequency components, with approximately the same intensity ratio, were observed in the spectrum of $CeRu_2$ synthesized at 5 GPa, though there was present also an about 30% contribution of a broad low-frequency distribution.

The narrowness of the frequency distributions and the absence of positions with intermediate values of the quadrupole frequency indicate that the nearest environments of the observed two sites occupied by the probe nuclei are electrically uniform, differing in quadrupole charge density at the ^{111}In/^{111}Cd sites.

To find out if the observed second site is due to the high-pressure effect, we tried to eliminate the latter by annealing one of the $CeRu_2$ samples prepared at 8 GPa. At first, the $CeRu_2$ sample was annealed in an argon atmosphere for several hours at 400 °C, but no changes were observed in the TDPAC spectrum; its significant modification was achieved by further treatment at 600°C for 3 h. Figure 5 demonstrates the spectra of the as cast and the annealed samples of $CeRu_2$. It is seen from the spectra and the data of their analysis presented in Table I that the lower-frequency component was transformed into a broad frequency distribution with a low average value of ν_Q, while the high-frequency component was left unchanged. The intensity ratio of the two components was the same (about unity) as in the initial spectrum; i.e., annealing induced certain changes only at the sites characterized by the low quadrupole frequency.

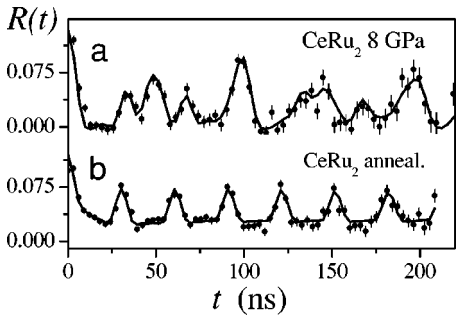

FIG. 5. ^{111}Cd-TDPAC spectra measured at room temperature and atmospheric pressure for (a) $CeRu_2$ synthesized at 8 GPa and (b) $CeRu_2$ synthesized at 8 GPa and annealed at 600 °C for 4 h.

The TDPAC spectra for the samples $Ce_{0.8}La_{0.2}Ru_2$ and $Ce_{0.4}La_{0.6}Ru_2$ are shown in Figs. 4(b) and 4(c), respectively, and their fitting parameters are presented in Table I. In the first case a two-component pattern, similar to $CeRu_2$ was observed, with slightly lowered relative contribution of the 152 MHz component. At higher concentration of La it vanished, and the spectrum reproduced that for pure $LaRu_2$, except a markedly higher value of the asymmetry parameter. This may be a result of the lattice constant variation with increasing lanthanum concentration mentioned in the Introduction.

Regular studies of EQI for ^{111}Cd in a series $Ce_{1-x}La_xRu_2$ are being completed and will be published elsewhere.

The results obtained show that in the $CeRu_2$ samples synthesized at high pressure there exist large enough regions where the nearest neighbors of the probe nuclei experience different quadrupole charge density at their sites. As long as the EXAFS results indicate that the Ce valence state is the same, independent of the method of synthesis and thermal treatment of the samples, this difference should be ascribed

TABLE I. EFG parameters for ^{111}Cd in $Ce_{1-x}La_xRu_2$ synthesized at 8 GPa.

	Site 1				Site 2			
Samples	ν_Q (MHz)	η	Λ	p	ν_Q(MHz)	η	Λ	p
$LaRu_2$	234(1)	0.03(2)	0.005(1)	0.95				
$Ce_{0.4}La_{0.6}Ru_2$	225(1)	0.13(1)	0.011(1)	0.90				
$Ce_{0.8}La_{0.2}Ru_2$	225(1)	0.13(1)	0.013(2)	0.50	152(1)	0.15(1)	0.014(4)	0.30
$CeRu_2$	218(1)	0.06(2)	0.000(3)	0.4	152(1)	0.11(2)	0.006(3)	0.45
$CeRu_2$ annealed (600 °C, 3 h)	217(1)	0.03(3)	0.004(3)	0.5	61(6)	0.0	0.7(2)	0.5

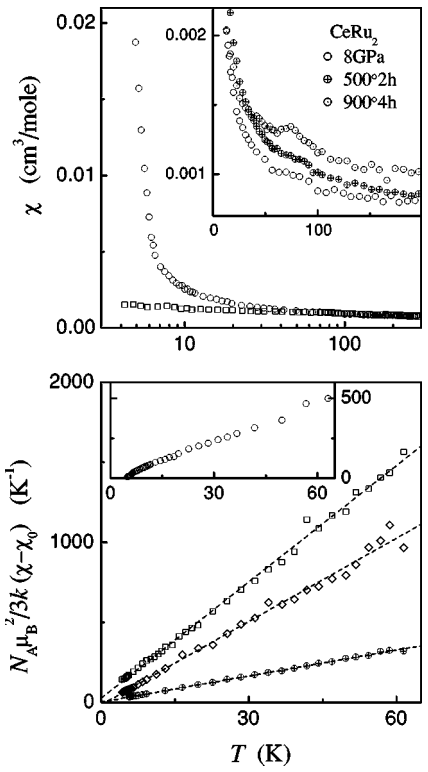

FIG. 6. Temperature dependences of the magnetic susceptibility measured at $H=300$ Oe for $Ce_{1-x}La_xRu_2$ synthesized at 8 GPa: ($\bigcirc,\oplus,\odot$) $CeRu_2$, ($\square$) $LaRu_2$, and ($\diamond$) $Ce_{0.75}La_{0.25}Ru_2$. In the insets $\chi(T)$ curves for $CeRu_2$ are presented on an enlarged scale. Dashed lines in the bottom panel represent fits of the experimental data by Eq. (4) with parameters χ_0, μ, and θ presented in Table II.

to certain differences in the electron configurations of Ru ions. The volumes of these regions should be large enough to make negligible the probability of populating by In/Cd impurities the sites in the boundaries between them, as the distributions of ν_Q values are very narrow.

Thus, in the process of $CeRu_2$ crystallization at high enough pressure certain changes in the $4d$-band structure occur as compared to the compound, prepared at normal conditions. Annealing influences in turn these changes and, as is shown in the next section, strongly affects the magnetic properties of the samples.

C. Magnetic correlations and superconductivity

Six samples of $CeRu_2$, two samples of $LaRu_2$, and several samples of intermediate compositions were investigated in magnetic measurements. The magnetic susceptibility χ was measured in a magnetic field of 300 Oe in the temperature range 5 K$\leqslant T\leqslant$300 K. Curie-Weiss-like behavior was observed for all samples, with an irregularity (a bump) at $T\sim$70–80 K. This irregularity became more prominent after annealing of the samples, as is illustrated for $CeRu_2$ in Fig. 6. The $\chi(T)$ curves follow the Curie-Weiss law

$$\chi=\chi_0+\frac{N_A}{3k}\frac{\mu^2}{T-\theta}. \tag{4}$$

Here χ_0 is the temperature-independent part of the susceptibility, μ is the effective magnetic moment per formula unit, θ is the Curie or Néel temperature, N_A is the Avogadro number, and k is the Boltzmann constant.

The values of χ_0, μ, and θ, obtained via fitting of $\chi(T)$ curves by Eq. (4) are presented in Table II. Note that in the temperature ranges below and above the irregularity the values of χ_0, μ, and θ are different, which obviously indicates certain changes in the electronic structure of the samples at $T\sim$70–80 K. A significant variation of these parameters was observed as a result of annealing in vacuum at a pressure of 10^{-6} torr.

It is seen from Table II that at low temperature the interaction of magnetic moments in $LaRu_2$ is antiferromagnetic while in $CeRu_2$ it is of ferromagnetic character.

At low temperature the magnetic moments tend to be correlated, and below the Curie or Néel temperature one would expect a setting up of the magnetic ordering. However, as the superconducting transition precedes a possible establishing of the magnetic ordering, we were unable to detect the latter. For example, $CeRu_2$ can be ferromagnetic at $T\lesssim$4.6 K while a superconducting transition occurs at $T_c=5.0$ K.

The temperature dependence of the magnetization M for the as-cast and annealed samples of $CeRu_2$ is shown in Fig. 7. At first the samples were cooled down in zero field, and then a magnetic field of 1 Oe was applied. After that the samples were heated (and the ZFC curve was recorded) and then cooled again (FC curve). To minimize the demagnetiza-

TABLE II. Magnetization parameters for $Ce_{1-x}La_xRu_2$ synthesized at 8 GPa.

	$T>80$ K			$T\leqslant 65$ K			
Samples	$\chi_0\times10^4$ (cm^3/mol)	μ (μ_B)	θ (K)	$\chi_0\times10^4$ (cm^3/mol)	μ (μ_B)	θ (K)	T_c (K)
$LaRu_2$	7.4(2)	0.4(2)	5(20)	9.4(1)	0.20(8)	−4(2)	<4.21
$LaRu_2$ annealed (520 °C, 4 h)	8.2(1)	0.3(2)	13(5)	10.3(2)	0.15(9)	−1(3)	<4.21
$Ce_{0.75}La_{0.25}Ru_2$				6.1(1)	0.24(4)	0.8(1)	<4.21
$Ce_{0.8}La_{0.2}Ru_2$				5.90(4)	0.22(4)	0.8(2)	<4.21
$Ce_{0.9}La_{0.1}Ru_2$				5.6(1)	0.26(7)	0.6(3)	<4.21
$CeRu_2$	6.0(5)	0.6(1)	−43(42)	9.1(2)	0.27(5)	4.58(3)	5.00(5)
$CeRu_2$ annealed (500 °C, 2 h)	6.6(1)	0.5(2)	5(8)	7.9(1)	0.43(6)	−0.2(1)	5.7(1)

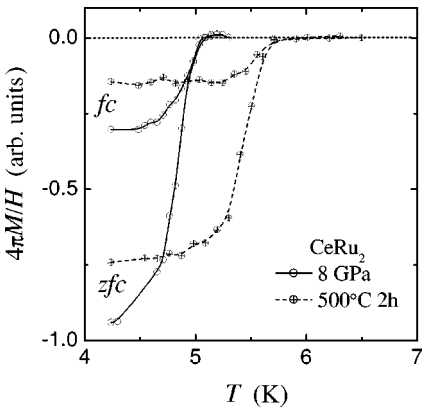

FIG. 7. Temperature dependences of the magnetization measured for $CeRu_2$ at $H=1$ Oe. For a detailed explanation see the text.

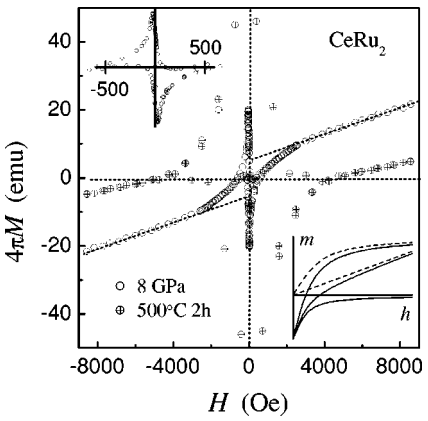

FIG. 8. Magnetization vs magnetic field measured for $CeRu_2$ at $T=4.25$ K. Dotted lines are the asymptotes of high-field magnetization. Low-field magnetization is presented in the top inset. Magnetization curves (solid line) for a superconductor with $H_{c1} \ll H_{c2}$ are shown in the bottom inset for different types of normal-state magnetization (dashed line). Bottom curve: ordinary dia/para magnetism. Middle curves: enhanced paramagnetism. Top curves: spin glass, ferromagnetism, or strong paramagnetism with Brillouin-like $m(h)$.

tion effect, the samples shaped into rods about 3 mm long and 0.3–0.5 mm thick were aligned along the applied magnetic field.

For the as-cast samples the critical temperature $T_c = 5.0$ K was obtained, which is significantly lower than $T_c = 6.2$ K for ordinarily prepared $CeRu_2$. Annealing at 500 °C for 2 h resulted in a substantial increase of T_c up to 5.7 K (see Fig. 7 and Table II), though it did not reach the above-cited normal value. Further annealing at 900 °C for 4 h has only slightly changed T_c.

All samples are characterized by a strong flux expulsion: The Meissner fraction was of the order of 30% of the as-cast sample volume (see Fig. 7). Annealing at 500 °C resulted in a reduction of the superconducting fraction down to about 75% of the sample volume but further annealing at 900 °C restored superconductivity in the whole sample. Strengthening of flux pinning was observed after each annealing step.

It should be stressed that the thermal treatment of the samples at 500°C could by no means induce any structural changes in their crystal structure.[47] Thus, the observed marked sensitivity of their superconductivity to annealing evidently reflects a certain variation of their electronic structure due to decay of the state formed in the conditions of high-pressure synthesis.

Magnetization curves for the as-cast and annealed at 500 °C samples measured in the field range $H \leqslant 9$ kOe are shown in Fig. 8. The curve for the as-cast sample is markedly nonlinear, and a slight hysteresis is observed at field values below 1 kOe. A similar behavior was observed for $Ce_{1-x}Gd_xRu_2$ with a few percent of Ce substituted by magnetic Gd ions.[48] The curve for the annealed sample is practically linear in the field range where the magnetization is reversible, which is also characteristic for monocrystalline $CeRu_2$.[49]

The sample normal-state magnetization affects the field dependence of their reversible magnetization. For illustration we present in the inset of Fig. 8 sketches of the magnetization curves for superconductors with different types of the normal-state magnetization. It is seen that in samples with negligibly small normal-state magnetization the high-field magnetization is negative and close to zero. For strongly paramagnetic superconducting material the high-field magnetization is positive, asymptotically approximating a straight line starting from zero, with a slope determined by the enhanced paramagnetic susceptibility. In the case of nonlinear normal-state magnetization the asymptote of the magnetization curve crosses the magnetization axis at a positive value.

In the field range used in our experiments we were unable to separate superconducting and magnetic contributions into the magnetization. However, analysis of the $M(H)$ curve for the as-cast sample of $CeRu_2$ testifies to a nonlinear field dependence of the normal-state magnetization. It should be stressed that in our case the interaction energy of magnetic moments with applied field is low, $\mu H \ll kT$, and insufficient for the moment ordering. Thus the nonlinear normal-state magnetization should be attributed to the interaction of the correlated moments with a molecular field induced by the moments themselves.

The results of the magnetic measurements allow us to state that in $Ce_{1-x}La_xRu_2$ synthesized at high pressure significant magnetic moments are formed which tend to be correlated at low temperature. In addition, the coexistence of magnetic ordering and superconductivity can also be proposed. These features radically differ from those of $CeRu_2$ prepared at an ambient pressure where the magnetic moments are about three orders of magnitude lower.[24,25]

If the estimated moments were related to the *f* states of Ce ions, their valent state should be different in samples prepared at high and low pressure. However, no difference was observed in our XAFS measurements and thus these magnetic moments should be associated with Ru sites. This assumption is corroborated by the existence of the moments in $LaRu_2$ where the *f* band is nearly empty.[16]

We have to discuss the probable influence of magnetic impurities on the magnetic properties of the samples studied.

The purity of the latter is determined by the purity of the ingredients (La, Ce, and Ru) claimed by the manufacturer and cited above. Assigning the measured magnetic moments $\mu \gtrsim 0.2\mu_B$ (see Table II) to a possible contamination we obtain $\mu \gtrsim 20\mu_B$ and $\mu \gtrsim 200\mu_B$ per an impurity atom in $LaRu_2$ and $CeRu_2$, respectively. The latter value is quite unrealistic, and the above assumption may be ruled out for the Ce-rich compounds $Ce_{1-x}La_xRu_2$, though it should be considered for the La-rich samples. The estimated value of μ positively excludes from consideration $3d$ and $4d$ impurities, and only heavy rare earths, which may possess magnetic moments as high as $10\mu_B$, should be taken into account.

To give rise to the observed magnetically correlated state in the $LaRu_2$ samples these impurity atoms have to create a segregated RRu_2 phase, which seems rather unlikely because of complete mutual solubility of the RRu_2 Laves compounds. At a comparatively low concentration the impurity rare-earth atoms would most probably prefer to substitute for La at random, as isolated paramagnetic ions forming, in turn, nonmagnetic Kondo impurity states. Thus, no magnetic correlations can be set up, and we may conclude that only a minor part, if any, of the magnetic moment observed for $LaRu_2$ may be attributed to rare-earth impurities and the major contribution is inherent in the high-pressure phase of $LaRu_2$ itself. Nevertheless, the magnetic data obtained for La-rich samples of $Ce_{1-x}La_xRu_2$ should be considered as preliminary, and measurements for higher-purity samples are necessary.

IV. DISCUSSION

The experimental data outlined above indicate that synthesis at high pressure of the Laves compounds $LaRu_2$ and, especially, $CeRu_2$ results in a significant modification of their electronic structure, whereas their crystal structure is left unchanged. Magnetic moments which tend to correlate at low temperature are formed in both compounds.

In $LaRu_2$ an about threefold increase of the temperature-independent susceptibility χ_0 and a notable decrease of the EFG at the $^{111}In/^{111}Cd$ impurity are observed as compared to samples prepared at ambient pressure. Since χ_0 is proportional to the density of states at the Fermi level $g(\varepsilon_F)$, the former means an increase of $g(\varepsilon_F)$.

In $CeRu_2$ the magnetic moments are three orders of magnitude higher than in the ''normal'' phase, the critical temperature is significantly lowered (5 K vs 6.2 K), two well-separated regions are observed where the impurity ^{111}Cd nuclei experience different and EFG's. It should be noted that lowering of T_c to 5 K was also observed at about 6 GPa in the *in situ* experiment.[32] Our data show that the pressure-induced variation of T_c is preserved at normal conditions and that the corresponding changes of the electronic structure are metastable: annealing at a moderately elevated temperature increased T_c, though did not restore it completely. The regions characterized by the low-frequency EFG component for ^{111}Cd are also metastable, and their destruction begins above 400 °C.

Here we shall try to qualitatively interpret these results in terms of the band structure for $LaRu_2$ and $CeRu_2$ calculated in Refs. 16–18 and 27.

In both compounds, the main contribution into the density of states on the Fermi level is formed by the ruthenium $4d$ states. The Fermi level ε_F is situated approximately at the half-maximum of the narrow peak of the density of $4d$ states, but in $LaRu_2$ it is above its maximum (i.e., higher in energy) and in $CeRu_2$ it is below it. In $CeRu_2$ the $4f$-electron density forms a broad peak above ε_F, and f electrons determine about 30% contribution into $g(\varepsilon_F)$. In $LaRu_2$ the $4f$ band is empty, and above the Fermi level lies the La band of the p-like states.[27]

Under pressure the energy of electron states increases, the energy shift for f and d states being larger than for s and p states. This may induce a redistribution of partial contributions into $g(\varepsilon_F)$ due to states with different orbital momenta and variations of the states population.

To minimize the system energy, electrons abandon states with high orbital momenta and populate those with lower momenta, provided the latter are present in the system. Evidently, this situation is realized in $LaRu_2$ whose Fermi level is shifted under pressure into the band of the La p-like states, and electrons partly abandon Ru d states and populate p states. Simultaneously, the peak of density of d states overlaps the Fermi level. As a result, the temperature-independent susceptibility χ_0, which is proportional to $g(\varepsilon_F)$, increases, as is observed in the experiment. The variation of the d-state population may be the cause of the about 8% difference observed in the EFG at ^{111}Cd measured in this work and by Devare *et al.*[45]

This situation seems to be similar to that observed earlier in the cubic Laves compound $GdNi_2$.[33] The EFG at the impurity nuclei ^{181}Ta at the substitutional sites in the Ni sublattice was found to be about 25% higher in samples synthesized at a pressure above 5 GPa than in ''normal'' samples. In a definite range of the synthesis pressure the coexistence of regions with two different values of the EFG was observed. This result was interpreted as being due to a decrease of the Ni $3d$-band filling in samples prepared at high pressure as compared to ''normal'' ones in which the $3d$ band is completely filled.

If the density of s and p states in the vicinity of ε_F is low, electrons cannot abandon f and d states, and the Fermi level is shifted to higher energy together with these states. The overall electron energy increases significantly, and the system will tend to decrease its energy by means of a certain electron or structural transition. Probably, such a process is developed in $CeRu_2$ where the partial density of sp states near the Fermi level is negligible.[16,17] In particular, the electronic structure rearrangement results in a sharp decrease of T_c mentioned in the Introduction and a jump of resistivity temperature coefficient observed by Hedo *et al.*[32] for $CeRu_2$ in the *in situ* measurements. High-pressure-induced variation of the critical temperature of the superconducting transition occurs as being irreversible; i.e., the metastable state formed in our samples is characterized by the same decreased value of T_c.

The most intriguing problem is that brought forward by

the observation of two distinct EFG's at ^{111}In/^{111}Cd sites in $CeRu_2$. The simplest explanation may be offered by the assumption of an admixture of an unknown crystal phase formed in the process of $CeRu_2$ solidification at high pressure. The abundance of this hypothetical phase should be low to be undistinguishable in x-ray experiments. On the other hand, the affinity of the indium impurity atoms to this phase should be so high that about a half of them is absorbed there. It should be also kept in mind that the ^{111}In/^{111}Cd concentration is far too low (about 10^{-8} at. %) to allow the formation of any separate intermetallic compounds with cerium or ruthenium. If a certain amount of indium was left in undissolved fraction of silver (see Sec. II C) or substituted for cerium, the EFG should be close to zero since in both cases it would reside at sites with cubic symmetry. A relatively small (5%–10%) constant background observed in the TDPAC spectra of $Ce_{1-x}La_xRu_2$ may be ascribed to these sites.

It should be stressed also that the low EFG component transformation by annealing is undoubtedly correlated with changes in the superconducting and magnetic properties, which could not be sensitive to the small admixture of an alien phase.

These considerations, as well as the observed dependence of the lower EFG component on La concentration in the quasibinary systems $Ce_{1-x}La_xRu_2$, make us to believe that attribution of this component to an alien crystal phase is unlikely.

Hence, we are to infer that the observed two values of quadrupole frequencies correspond to ^{111}In/^{111}Cd impurities substituting for Ru in a unique $C15$ crystal phase. As long as the XANES measurements have shown that the Ce valence is independent of the method of synthesis and thermal treatment of the samples, the positions with different electric quadrupole charge densities at the impurity sites should differ in the electronic configurations of the nearest Ru ions.

A rather small width of the frequency distributions means that regions characterized by a certain value of ν_Q are sufficiently large and well segregated to make negligible the probability for probe atoms to find the nearest Ru ions with different electronic configurations.

To understand the formation of regions with different electronic configurations of the Ru ions in $CeRu_2$ synthesized at high pressure, additional experimental and theoretical data are necessary. Qualitatively, it may be the result of a high density of states at the Fermi level which is higher than that in isostructural compounds $LaRu_2$ and $CeRh_2$.[16] The latter has one extra $4d$ electron per each rhodium ion as compared to $CeRu_2$. In $CeRh_2$ the completely filled $4d$ band lies below the Fermi level, and the main contribution to $g(\varepsilon_F)$ stems from the Ce $4f$ electrons.[16] As was mentioned above, in $LaRu_2$ the $4f$ band is empty and the Fermi level is situated at the peak of the density of the $4d$ states.[16] To gain energy stability and to decrease $g(\varepsilon_F)$ at high pressure, an electron transition may occur in $CeRu_2$ proceeding in two ways and leading to the formation of $LaRu_2$-like and $CeRh_2$-like regions where the Ru ions find themselves in different electronic configurations or, in other words, in different effective charge states.

In conclusion we state that in the studied quasibinary systems $Ce_{1-x}La_xRu_2$ synthesized at high pressure magnetic moments are formed on the Ru ions, which are involved in an exchange interaction. On the other hand, the ruthenium d states significantly contribute to the sample superconductivity. Thus, $Ce_{1-x}La_xRu_2$ represents a system where magnetic and superconducting correlations develop in a common electron system, which represents a special interest from the fundamental point of view.

For the creation of a more reliable and detailed model of the electron structure of the high-pressure phase of $Ce_{1-x}La_xRu_2$ additional studies of the low-temperature specific heat, magnetic structure, and temperature dependence of the superconducting gap are necessary, as well as refined band structure calculations taking into account pressure effects. The latter are especially important for the explanation of two different electronic configurations of Ru ions in $CeRu_2$.

ACKNOWLEDGMENTS

The authors acknowledge Professor E. Maksimov and Dr. A. Sinchenko for helpful discussions of the results. We are also indebted to Dr. D. Eremenko and Dr. P. Konarev for assistance in the experiments. The work was supported by Grant No. 01-02-97010, 99-02-17897, and 02-02-16942 of RFBR, and the program ''Superconductivity'' of the Russian Ministry of Science and Federal program ''Integration.''

[1] D.D. Koelling, B.D. Dunlap, and G.W. Crabtree, Phys. Rev. B **31**, 4966 (1985).
[2] V.V. Moshchalkov and N.B. Brandt, Usp. Fiz. Nauk **149**, 585 (1986); N.B. Brandt and V.V. Moshchalkov, Adv. Phys. **33**, 373 (1984).
[3] D.I. Khomski, Usp. Fiz. Nauk **129**, 443 (1979); J.M. Lawrence, P.S. Riseborough, and R.D. Parks, Rep. Prog. Phys. **44**, 1 (1981).
[4] G.R. Stewart, Rev. Mod. Phys. **56**, 755 (1984).
[5] D.D. Koelling, Physica B **130**, 135 (1985).
[6] M. Brian Maple, Physica B **215**, 110 (1995).
[7] F.U. Hillebrecht, J.C. Fuggle, and Z. Zołnierek, R. Lässer, Ch. Freiburg, O. Gunnarsson, and K. Schönhammer, Phys. Rev. B **27**, 7330 (1983).
[8] D. Wohlleben and J. Röhler, J. Appl. Phys. **55**, 1904 (1984).
[9] J. Garcia, A. Marcelli, M. Sanchez del Rio, J. Bartolome, D. Fruchart, S. Miraglia, and F. Vaillant, Physica B **158**, 521 (1989).
[10] J. Chaboy, J. Garcia, and A. Marcelli, J. Magn. Magn. Mater. **104-107**, 661 (1992).
[11] J.W. Allen, S.-J. Oh, I. Lindau, M.B. Maple, J.F. Suassuna, and S.B. Hagström, Phys. Rev. B **26**, 445 (1982).
[12] J.W. Allen, S.-J. Oh, M.B. Maple, and M.S. Torikachvili, Phys. Rev. B **28**, 5347 (1983).

[13] T. Nakama *et al.*, J. Phys. Soc. Jpn. **62**, 4129 (1993).
[14] S.-H. Yang, H. Kumigashira, T. Yokoya, A. Chainai, T. Takahashi, H. Takeya, and K. Kadowaki, Phys. Rev. B **53**, R11 946 (1996).
[15] J.-S. Kang, C.G. Olson, M. Hedo, Y. Inada, E. Yamamoto, Y. Haga, Y. Onuki, S.K. Kwon, and B.I. Min, Phys. Rev. B **60**, 5348 (1999).
[16] A. Yanase, J. Phys. F: Met. Phys. **16**, 1501 (1986).
[17] Masahiko Higuchi and Akira Hasegawa, J. Phys. Soc. Jpn. **65**, 1302 (1996).
[18] S. Tanaka, H. Harima, and A. Yanase, J. Phys. Soc. Jpn. **67**, 1342 (1998).
[19] M. Hedo, Y. Inada, T. Ishida, E. Yamamoto, Y. Haga, Y. Onuki, M. Higuchi, and A. Hasegawa, J. Phys. Soc. Jpn. **64**, 4535 (1995); M. Hedo, Y. Inada, K. Sakurai, E. Yamamoto, Y. Haga, Y. Onuki, S. Takahashi, M. Higuchi, M. Maehira, and A. Hasegawa, Philos. Mag. B **77**, 975 (1998).
[20] R.R. Joseph, K.A. Gschneider, Jr., and D.C. Koskimaki, Phys. Rev. B **6**, 3286 (1972).
[21] A.D. Huxley, P. Paulsent, O. Laborde, J.L. Tholence, D. Sanchez, A. Junod, and R. Calemczuk, J. Phys.: Condens. Matter **5**, 7709 (1993).
[22] M. Hedo, Y. Inada, E. Yamamoto, Y. Haga, Y. Onuki, Y. Aoki, T.D. Matsuda, H. Sato, and T. Takahashi, J. Phys. Soc. Jpn. **67**, 272 (1998).
[23] T. Nakama, M. Hedo, T. Maekawa, M. Higa, R. Resel, H. Sugawara, R. Settai, Y. Onuki, and K. Yagasaki, J. Phys. Soc. Jpn. **64**, 1471 (1995).
[24] A.D. Huxley, P. Dalmas de Reytier, A. Yaouanc, D. Caplan, M. Couach, P. Lejay, P.C.M. Gubbens, and A.M. Mulders, Phys. Rev. B **54**, R9666 (1996).
[25] A. Huxley, J.X. Boucherie, M. Bonnet, F. Bourdarot, I. Schustler, D. Caplan, E. Lelievre, N. Bernhoeft, P. Lejay, and B. Gillon, J. Phys.: Condens. Matter **9**, 4185 (1997).
[26] E.D. Isaacs, D.B.Mc. Whan, R.N. Kleiman, D.J. Bishop, G.E. Ice, P. Zschack, B.D. Gaulin, T.E. Mason, J.D. Garrett, and W.J.L. Buyers, Phys. Rev. Lett. **65**, 3185 (1990); T.E. Mason, B.D. Gaulin, J.D. Garrett, Z. Tun, W.J.L. Buyers, and E.D. Isaacs, *ibid.* **65**, 3189 (1990); G. Aeppli, E. Bucher, C. Broholm, J.K. Kjems, J. Baumann, and J. Hufnagl, *ibid.* **60**, 615 (1988).
[27] R. Asokamani, G. Subramoniam, S. Mathi Jaya, and S. Pauline, Phys. Rev. B **44**, 2283 (1991).
[28] S. Chudinov, M. Brando, A. Marcelli, and M. Battisti, Physica B **244**, 154 (1998).
[29] R.N. Shelton, A.C. Lawson, and K. Barberchke, Solid State Commun. **24**, 465 (1977).
[30] T. Nakama, Y. Uwatoko, T. Kohama, A.T. Burkov, Y. Yamaguchi, H. Yoshida, S. Abe, T. Kaneko, N. Môri, and K. Yagasaki, J. Magn. Magn. Mater. **177–181**, 425 (1998).
[31] D. Groten, E. Ardonne, S. Ramakrishnan, G.J. Nieuwenhuys, and J.A. Mydosh, Physica C **306**, 271 (1998).
[32] M. Hedo, T. Tanaka, A.T. Burkov, K. Yagasaki, Y. Uwatoko, H. Takahashi, T. Nakanishi, and N. Mori, Physica B **281&282**, 88 (2000).
[33] A.V. Tsvyashchenko, L.N. Fomicheva, E.N. Shirani, A.A. Sorokin, G.K. Ruasny, B.A. Komissarova, L.G. Shpinkova, Z.Z. Akcelrod, O.I. Kochetov, and V.N. Trofimov, Phys. Rev. B **55**, 6377 (1997).
[34] A.V. Tsvyashchenko, J. Less-Common Met. **99**, L9 (1984).
[35] L.G. Khvostantsev, L.F. Vereshchagin, and A.P. Novikov, High Temp.-High Press. **9**, 637 (1977).
[36] V.N. Trofimov, Cryogenics **32**, 513 (1992).
[37] P.A. Lee, P.H. Citrin, P. Eisenberger, and B.M. Kincaid, Rev. Mod. Phys. **53**, 769 (1981).
[38] A.L. Ankudinov, B. Ravel, J.J. Rehr, and S.D. Conradson, Phys. Rev. B **58**, 7565 (1998).
[39] R.M. Steffen and K. Alder, in *Extranuclear Perturbations of Angular Distributions and Correlations, The Electromagnetic Interaction in Nuclear Spectroscopy*, edited by W.D. Hamilton (North-Holland, Amsterdam, 1975), Chap. 13.
[40] *X-ray Absorption: Principles, Applications, Techniques of EXAFS, SEXAFS, and XANES*, edited by D.C. Koningsberger and R. Prince (Wiley, New York, 1988).
[41] Such a cluster corresponds to the first two coordination shells. We have checked out that additional coordination shells give a negligibly small correction to the calculation results.
[42] Jusús Chaboy, Augusto Marcelli, Latchezar Bozukov, Francois Baudelet, Elisabeth Dartyge, Alain Fontaine, and Stefania Pizzini, Phys. Rev. B **51**, 9005 (1995).
[43] J.W. Cook, Jr. and D.E. Sayers, J. Appl. Phys. **52**, 5024 (1981).
[44] E. Sevillano, H. Meuth, and J.J. Rehr, Phys. Rev. B **20**, 4908 (1979).
[45] S.H. Devare, H.G. Devare, S. Scholtz, L. Freize, and M. Forker, Hyperfine Interact. **15/16**, 629 (1983).
[46] In Ref. 45 the samples were synthesized at an ambient pressure and ^{111}In was diffused at 800 °C for 15 h.
[47] W. Obrowski, Z. Metallkd. **53**, 736 (1962).
[48] R.M. Bozorth, D.D. Davis, and A.J. Williams, Phys. Rev. **119**, 1570 (1960).
[49] Kazuo Kadowaki, Hiroyuki Takeya, and Kazuto Hirata, Phys. Rev. B **54**, 462 (1996).
[50] *Handbook on the Physics and Chemistry of Rare Earths*, edited by Karl A. Gschneidner, Jr. and Le Roy Eyring (North-Holland, Amsterdam, New York, 1978).